Published in final edited form as:
J Biomed Mater Res A. 2013 May ; 101(5): 1255–1264. doi:10.1002/jbm.a.34420.

3D Bioprinting of Heterogeneous Aortic Valve Conduits with Alginate/Gelatin Hydrogels

Bin Duan, **Laura A. Hockaday**, **Kevin H. Kang**, and **Jonathan T. Butcher***
Department of Biomedical Engineering, Cornell University, Ithaca, NY, USA

Abstract

Heart valve disease is a serious and growing public health problem for which prosthetic replacement is most commonly indicated. Current prosthetic devices are inadequate for younger adults and growing children. Tissue engineered living aortic valve conduits have potential for remodeling, regeneration, and growth, but fabricating natural anatomical complexity with cellular heterogeneity remain challenging. In the current study, we implement 3D bioprinting to fabricate living alginate/gelatin hydrogel valve conduits with anatomical architecture and direct incorporation of dual cell types in a regionally constrained manner. Encapsulated aortic root sinus smooth muscle cells (SMC) and aortic valve leaflet interstitial cells (VIC) were viable within alginate/gelatin hydrogel discs over 7 days in culture. Acellular 3D printed hydrogels exhibited reduced modulus, ultimate strength, and peak strain reducing slightly over 7-day culture, while the tensile biomechanics of cell-laden hydrogels were maintained. Aortic valve conduits were successfully bioprinted with direct encapsulation of SMC in the valve root and VIC in the leaflets. Both cell types were viable (81.4±3.4% for SMC and 83.2±4.0% for VIC) within 3D printed tissues. Encapsulated SMC expressed elevated alpha-smooth muscle actin when printed in stiff matrix, while VIC expressed elevated vimentin in soft matrix. These results demonstrate that anatomically complex, heterogeneously encapsulated aortic valve hydrogel conduits can be fabricated with 3D bioprinting.

Keywords

tissue engineering; interstitial cell; smooth muscle; biomechanics; cell encapsulation

Introduction

Heart valves ensure critical one-way blood flow through the cardiovascular system. The aortic valve is particularly important, as it directs blood through the aorta and coronary arteries. Efficiency of valve performance is controlled by its complex anatomical geometry and heterogeneous tissue biomechanics.[1] Congenital malformations and/or acquired valve diseases compromise valve shape and/or tissue mechanics, leading to the narrowing of valve orifice area (stenosis) or leaking (regurgitation). Aortic valve disease is a significant cause of morbidity and mortality.[2] While the aortic valve can sometimes be surgically repaired, prosthetic replacement is only option for the vast majority of patients.[3] Mechanical valves are durable but suffer risks of clot formation on their prosthetic surfaces, necessitating life-long anti-coagulant drug therapy. Bioprosthetic valves, on the other hand, have minimal risk for bleeding events but are much less durable and unsuitable for pediatric applications.[3,4] The pulmonary autograft, or Ross procedure, is an attractive option to provide a living valve

*Corresponding author: Department of Biomedical Engineering, Cornell University, Ithaca, NY, USA. jtb47@cornell.edu.
The authors have no financial disclosures.

in the aortic position, but recent studies suggest that the pulmonary conduit may pathologically dilate, particularly in growing children.[5] Tissue engineering is a promising alternative strategy with the potential to provide a living valve replacement capable of integration with host tissue and growth.[6] A common fabrication process is to mold a valve shape from a biodegradable scaffold material, seed it with cells, and culture it *in vitro*, often under dynamic stimulation, before implantation.[7-11] A wide range of synthetic polymers, such as polyglycolic acid and poly-4-hydroxybutyrate, and natural biomaterials such as fibrin and collagen have been employed to generate 3D heart valve scaffolds.[9,12-14] Electrospinning has been utilized to create nanofibrous membranes that exhibit anisotropic biomechanical properties like that of the native valve leaflet.[15,16] However, few attempts have been made to engineer heart valve conduits (root and integrated leaflets). Using molds necessitates a single material formulation (and the same cell type if included) for both valve root and leaflets and thus creates homogeneous material biomechanics. This approach risks creating root walls that are too compliant or cusps that are too stiff. Even complex mold shapes have significant challenges to replicate valve sinuses and coronary ostia, which are important for optimal hemodynamic performance.[17]

Bioprinting approaches employing layer-by-layer additive fabrication technology have recently been employed to produce three-dimensional (3D) biological materials that exhibit high resolution geometric and/or mechanical complexity, including inkjet bioprinting, laser assisted bioprinting, and 3D bioprinting.[18,19] 3D bioprinting implements rapid prototyping (RP) techniques, which follows computer-assisted design (CAD) and/or computer-assisted manufacturing (CAM) blueprints to build a complex tissue construct.[20] Several studies have demonstrated the capacity of 3D bioprinting to fabricate 3D structures for various tissue regeneration applications or biomedical devices, including knee menisci, blood vessels, and liver.[21-23] Most hydrogel bioprinting studies to date have fabricated relatively simple slabs or self supporting structures that are unsuitable for the geometric complexity of heart valves.[22,24] Stereolithography based printing can create intricate 3D shapes, but the fabrication process is cyotoxic. Conversely, two-photon laser based photocrosslinking can create directly encapsulated 3D tissues with high spatial resolution, but only a few millimeters in overall size, which is clinically inadequate.[25,26] Recently, new biomaterials with capacity for photopolymerization or thermosensitivity have been adapted for 3D bioprinting, including A-B-A triblock copolymer hydrogel composed of poly(*N*-(2-hydroxypropyl)methacrylamide lactate) A-blocks, partly derivatized with methacrylate groups, and hydrophilic poly(ethylene glycol) B-blocks,[27] and hydroxyethyl-methacrylate-derivatized dextran (dex-HEMA).[24] Hybrid tissue fabrication strategies are also possible through alternating deposition of thermoplastic materials and cell-laden hydrogels.[28] 3D bioprinting may therefore be a promising technology for rapid fabrication of intrinsically complex, cell encapsulated aortic valve conduits.

In this study, we test the ability for 3D bioprinting to utilize alginate/gelatin hydrogel formulations to fabricate living heterogeneous aortic valve conduits. We quantify 3D printing accuracy, printed and evolved tissue biomechanics, and cell differentiation.

Materials and Methods

Cell isolation

Porcine aortic valves were obtained at a slaughterhouse (Shirk Meats, Himrod NY). Porcine aortic valve interstitial cells (VIC) were isolated via collagenase digestion of the leaflets after endothelial cells were removed as previously described.[29] Human aortic root smooth muscle cells were isolated from the aortic root of a 12 year old young patient while undergoing cardiac transplant for a non-valve problem. The aortic root was inspected to be grossly normal. Tissue was procured with consent as approved by the Institutional Review

Board of Weill-Cornell Medical College in New York City. Cells were cultured in Dulbecco's Modified Eagle's Medium (DMEM; Invitrogen, Carlsbad, CA) supplemented with 10% fetal bovine serum (FBS; Invitrogen) and 1% penicillin/streptomycin (P/S; Invitrogen). Cells were used at passages 5-8.

Hydrogel preparation

Gelatin (porcine skin Type A, Sigma) was dissolved at 0.06 g/ml in sodium chloride solution under constant stirring at 40 °C. Then 0.05 g/ml of alginate (non-medical grade LF10/60 alginate, FMC BioPolymer, Drammen, Norway) was dissolved into gelatin solution. For cell encapsulation, VIC and SMC were mixed into separate alginate/gelatin gel solutions at densities of 2×10^6 cells/ml. Each cell laden alginate/gelatin gel was loaded into syringe and directly extruded into disc molds (Ø8 mm×1mm). The resultant alginate/gelatin gel discs were then ionically crosslinked by calcium chloride ($CaCl_2$, 300 mM, Sigma) for 5 min. Gelatin was gradually released from ionically crosslinked hydrogel discs detected by BCA (bicinchoninic acid) Protein Assays (Pierce) (Supplemental Figure S1).

Bioprinting of 3D constructs

Three different 3D geometries were designed and printed. First, square grid patterns were first designed to evaluate accuracy of 3D printing with alginate/gelatin. A grid pattern was designed and converted into vector file format, as shown in Fig. 5A. The distance between each printed line is 2 mm. We measured the channel dimensions in both X and Y directions and the printing accuracy was assessed by comparing the measured channel area to the design value (4 mm^2) using following equation:

$$\%\text{Accuracy}=\left[\frac{1}{n}\sum_{i=1}^{n}\left(1-\frac{|A_i-A|}{A}\right)\right]\times 100\%$$

where A_i is measured channel area, A is design area (4 mm^2) and n represents total number of channel in a printed construct. Three printed constructs were used for the printing accuracy test. Next, a dumbbell-shaped model was designed and fabricated to determine mechanical properties of cell-free 3D printed alginate/gelatin hydrogels. We designed an 80% scaled version of ASTM D638-10 Type V, with thickness of 3.20 mm; width of 2.54 mm, gage length of 6.10mm, and 20.32mm distance between grips. This was converted into stereolithography (STL) format and imported into the 3D bioprinter software.

For the 3D aortic valve model, freshly harvested porcine aortic valves (Shirk Meats, Himrod, NY) were rinsed with sterile PBS, preserved in formalin, and then scanned using micro-CT (GE eXplore CT120; GE Health Care, Milwaukee, WI) at 100 μm resolution, 80 keV, 30 mA, 800 angles, 30 ms exposure time, 30 gain, and 20 offset.[30] The root and leaflet regions in the scans were identified with intensity thresholds and rendered separately into 3D geometries into STL format (Fig. 6A green for root and red for leaflet).[31]

The Fab@Home™ open-source, open-architecture RP platform (www.fab@home.org) was used for printing the alginate/gelatin gels. The vector file (for 3D grid patterned bioprinting) and STL file (for bioprinting of dumbbell-shaped tensile test samples and living aortic valve conduit) were imported into the printer. The software converted the imported STL file into print paths by slicing them into layers and generating contour and fill-paths for each layer based on specific print parameters.[31] The standard print head was modified to incorporate three linear actuator-driven deposition tools with interchangeable syringe tips with inner diameter of 800 μm (EFD Inc, East Providence, RI) that can be positioned on the XY plane

with 25 μm precision. Alginate/gelatin hydrogel formulations were then loaded aseptically into the deposition syringes. Gels were extruded along the X-Y target paths for each layer, and after each layer completed the print stage in was translated Z (for 3D aortic valve model), thus sequentially building the construct. The standard printing parameters used in our experiments were 0.8 mm path width, 0.7 mm path height, and 5 mm/s path speed. SMC or VIC were mixed into the alginate/gelatin gel at a density of 1×10^7 cells/ml. Only one cell type (VIC) was encapsulated within the printed 3D square grid patterns or dumbbell-shaped tensile test samples. Both cell types (SMC for the root and VIC for the leaflets) were encapsulated in the bioprinted aortic valve conduits. Each cell type was mixed in its own hydrogel and contained in separate syringes. The printer software controlled extrusion from each syringe so that the root section of each layer was fabricated first, followed by the leaflet component. After each print was completed, the final structures were then ionically crosslinked in $CaCl_2$ (300 mM) for 10 min.

Tensile biomechanics tests

Uniaxial tensile properties of printed and ionically crosslinked cell-free and cell encapsulated dumbbell-shaped hydrogels were tested after 0, 1, and 7 days culture using an ELF 3200 (EnduraTec) mechanical test-frame. A 1 kg load cell (Sensotec) with 2 g resolution was attached to the bottom plate and a displacement sensor to the top plate. The cross-head speed was 0.075 mm/s and the gauge length was about 20 mm. Load data were acquired at a frequency of 5 Hz, and displacement and load data were converted to strain and stress, respectively, by normalizing to sample thickness and area.

Cell viability and spreading in gels

The viability of encapsulated cells was determined using Live/Dead and MTT cell viability assays (Invitrogen) according to manufacturer's instructions. For Live/Dead assay, fluorescence images were obtained immediately using a confocal microscopy (CLSM, LSM 710, Carl Zeiss). Cell viability was measured via counting live (green) and dead (red) cells using ImageJ. The MTT assay was conducted on VIC and SMC encapsulated in alginate/gelatin hydrogel discs at both low (2×10^6 cells/ml) or high cell density (1×10^7 cells/ml).

SMC and VIC were incubated for 30 minutes with CellTracker™ Green CMFDA and CellTracker™ Red CMPTX (Invitrogen), respectively. The 3D bioprinted constructs with cell tracker labeled cells were imaged after crosslinking. Cell spreading and circularity was quantified via ImageJ (Analyze Particles feature) by measuring the average surface area per cell and cell shape as previously described (Butcher et al 2004). Circularity ranges from 0 to 1, with 1 indicating a perfect circle and 0 a straight line.

Cell phenotype analysis

Cultured cell laden hydrogels were fixed by 4% paraformaldehyde in PBS for 4 h at 4 °C, permeabilized in 0.2% Trion X-100 for 10 min at room temperature, and blocked with 1% bovine serum albumin (BSA) overnight at 4 °C. To visualize actin cytoskeletal filaments, the hydrogels were stained by Alexa Fluor 488 conjugated phalloidin (1:40, Invitrogen). Hydrogels were also treated with primary antibodies to alpha smooth muscle actin (αSMA) (1:100, rabbit monoclonal anti-αSMA, Spring Biosciences), vimentin (1:100, mouse monoclonal anti-vimentin, Invitrogen), or type I collagen (Col1A2, 1:100, Santa Cruz Biotechnology), each overnight at 4 °C. Vimentin is expressed by fibroblasts and other mesenchymal cells, while αSMA is a contractile filament primarily in SMC.[32,33] Secondary fluorescent antibodies and nuclear counterstaining (via Draq 5, 1: 1000, Biostatus) were performed for 30 minutes at room temperature. Samples were imaged with Zeiss 710 CLSM as before. Protein expression was quantified as area of staining intensity above a threshold using ImageJ as previously described. [34,35,36]

Statistical analysis

All quantitative data are expressed as the mean±standard (SD). Six images were analyzed for each hydrogel sample (hydrogel disc or bioprinted hydrogel valve conduit). Four to six printed cell-free hydrogel samples and three cell-loaded samples were used for tensile testing, while 6 gels were used for cell morphometry and phenotype image analysis. Statistical analysis was performed using ANOVA with Scheffé post-hoc tests. A value of $p<0.05$ was considered to be statistically significant and $p<0.01$ remarkably significant.

Results

Cell encapsulation within hydrogel discs

VIC and SMC encapsulated within alginate/gelatin hydrogel discs were viable at both 1 and 7 days (Fig. 1A ,B). Cell viability for the encapsulated VIC was 91.2±5.7% at day 1 (Fig. 1C). Most VIC were not spread 1 day after printing, but maintained spherical morphology (circularity of 0.90±0.15). There was no change in VIC viability at day 7 (86.0±4.6%, p=?), but cells were significantly more spread with decreased circularity (0.76±0.21, $p<0.05$). The projected cell area of VIC increased from 127.1±99.4 μm at day 1 to 201.4±178.1μm at day 7 (Fig. 1D). Similarly, high cell viability for SMC encapsulation was maintained in culture (90.7±3.0% for 1 day and 84.6±5.1% for day 7, Fig. 2A-C). SMC projected cell area and spreading both significantly increased over the culture period (circularity of 0.91±0.06 for day 1 and 0.80±0.17 for day 7, $p<0.05$.), but SMC were less spread than VIC overall.

Cytoskeleton F-actin of encapsulated VIC and SMC was performed after 7 day culture (Fig. 3A). The encapsulated VIC were more extensively spread after 7 day culture. As shown in Fig. 3B, the encapsulated VIC express both αSMA and vimentin, but the expression of vimentin was significantly higher than αSMA expression, suggesting a more fibroblastic than myofibroblastic phenotype. The expression trends for SMC were reversed: αSMA was significantly higher than vimentin (Fig. 3D). αSMA staining was more diffuse than organized fibrils, which was not surprising given their limited spreading after 7 days culture.

Hydrogel tensile biomechanics

Alginate/gelatin hydrogels exhibit mostly linear stress-strain behavior, with significant extensibility and mechanical strength (Fig. 4A). The ultimate tensile strength in cell-free hydrogels decreased from 0.84±0.07 MPa to 0.64±0.12 MPa after 24 hours, and further decreased to 0.40±0.04 MPa after 7 days immersion (P<0.05, Fig. 4C). Similarly, the elastic modulus decreased from 1.44±0.30 MPa to 0.99±0.14 MPa after 24 hours (P<0.05), but this stiffness was maintained out to 7 days (0.96±0.08 MPa, Fig. 4E).

The ultimate tensile strength and failure strain for hydrogels encapsulated with VIC were 0.35±0.06 MPa and 38.76±3.82% respectively, significantly decreased compared to cell-free hydrogels ($p<0.01$). However, there was no significant difference in hydrogel modulus with and without cells at day 0. However, the tensile mechanics of cell-laden hydrogels did not change over culture, becoming statistically equivalent to cell-free samples after 7 day incubation (Fig. 4B-E). This is partly explained by the secretion of extracellular matrix proteins by encapsulated cells, including type I collagen (Fig. 4F).

Bioprinting of 3D patterned constructs

A simple 3D structure with grid type pattern was first designed and printed, as shown in Fig. 5A. The alginate/gelatin hydrogel with encapsulation of VIC maintained its geometry and mechanical integrity after extrusion and crosslinking (Fig. 5B). The printing accuracy (percentage overlap of printed to designed area) was 84.3±10.9%. Cells were evenly distributed throughout the printed tissue (Fig. 5C,D). Cell viability after 7 days culture was

determined via Live/Dead staining to be 84.6±3.1% (Fig. 5E). These results support the printability of alginate/gelatin hydrogel with good fidelity of defined geometries and high encapsulated cell viability.

Bioprinting of heterogeneous aortic valve conduits

SMC and VIC were encapsulated within separate alginate/gelatin hydrogel preparations. Fig. 6A shows the 3D model of porcine aortic valves reconstructed from micro-CT images. The leaflet and root regions were thresholded based on tissue density and reconstructed into two printable STL geometries (green for root and red for leaflet) and input into the Fab@Home™ system for bioprinting. A schematic diagram of the dual cell type bioprinting process is shown in Fig. 5B and C for the root and leaflet regions of the first layer. Using the dual-syringe Fab@Home bioprinter, the root (SMC laden hydrogel) was deposited first and subsequently, the leaflet region of the layer (VIC laden hydrogel) was extruded along its print paths. These steps were repeated for the subsequent layers to yield a 3D construct with the desired architecture and heterogeneous cell distributions. Valves were printed with low (2×10^6 cells/ml) or high cell density (1×10^7 cells/ml). Heterogeneous cell distribution in printed tissue layers was verified by fluorescent labeling (Fig. 6D). The 3D printed aortic valve conduit, complete with SMC and VIC encapsulated in the root and leaflet tissue, respectively, exhibited geometry comparable to the original image derived valve (Compare Fig. 6A and 6E). Key anatomical features, including sinuses and coronary ostia, were recapitulated faithfully. After 7 days additional culture, SMC encapsulated within the root had viability of 81.4±3.4%, while encapsulated VIC had viability of 83.2±4.0%. Unlike within hydrogel discs, the cells were less spread (148.8±99.6 μm^2 for VIC and 130.9±108.7 μm^2 for SMC) in the printed constructs. Both VIC and SMC expressed αSMA and vimentin protein after 7 days culture. VIC showed significant higher vimentin expression than αSMA (Fig. 7B), whereas SMC expressed more αSMA (Fig. 7D). These results confirm the feasibility of 3D bioprinting for heterogeneous cell encapsulated clinically sized tri-leaflet heart valves.

Discussion

3D bioprinting has great potential to fabricate heterogeneous tissues with multiple cell types, biohybrid materials and/or different mechanical properties, all of which are critical for the advancement of tissue engineering.[22,52] For example, aortic heart valve function is heavily dependent on its geometry and material composition. Engineering living tri-leaflet valves with anatomical and/or mechanical heterogeneity has been challenging with current fabrication strategies. In this study, we fabricated living aortic valve conduits with anatomical resemblance to the native valve based on alginate/gelatin hydrogel system via 3D bioprinting. Aortic valve root cells (SMC) and leaflet cells (VIC) were encapsulated within alginate/gelatin hydrogel and bioprinted in a dual syringe system to mimic the structure of valve root and leaflet, respectively. Various bioprinting machines based on deposition technique have been used for formation of 3D constructs. Most studies focused on homogenous 3D bioprinting with single material and single cell type.[41,51] We evaluated print accuracy in simple grid patterns as a means to rapidly optimize hydrogel formulation without having to print the whole valve. Both overall shape and internal pore structure were well preserved after bioprinting and further crosslinking. Both bioprinting parameters and hydrogel properties can affect the shape fidelity. Although we optimized the parameters for printing of alginate/gelatin hydrogel, the printing process paused at the end of each path for very short time, and the hydrogel was not totally sucked back, resulting in over extrusion at those locations. Therefore, the fidelity at central printed region was better than that at the edge region. More advanced determination of printing fidelity can be achieved using

recently developed 3D shape comparison algorithms that compare directly against 3D image data (Ballyns et al AND Laura's new paper).

Alginate is a naturally occurring anionic polymer with many attractive features for biomedical applications, including low cost, excellent biocompatibility, low toxicity, and a variety of crosslinking and biomolecular tethering flexibililty.[37] Alginate based hydrogels have been widely studied and used in wound healing, drug delivery, cell transplantation and tissue engineering, [38,39] but are also particularly attractive for bioprinting (both laser assisted bioprinting and 3D bioprinting) due to its broad range of viscosities at room temperature.[40-42] This is important, as hydrogels have tight requirements with regard to viscosity and gelling speed for accurate printing. Forming a hydrogel with an alginate/gelatin combination required decreasing the temperature from 37 °C to room temperature due to thermoreversibility of gelatin. The shear storage and loss moduli (G' and G'') of alginate/gelatin significantly increased during gelation process indicating the increase of viscosity.[43] There are two roles that gelatin plays in these 3D printed tissues. First, gelatin alters the viscosity of the hybrid hydrogel to enable extrusion and printing. Approximately 40% of the initial gelatin was present in the gel immediately after crosslinking, and about 20% of that was maintained in the gels over the 7 day period. This remnant gelatin may support cell adhesion and spreading. We employed different alginate/gelatin combinations during preliminary experiments. We found that with increasing proportion of alginate, the deposited hydrogel blend spread unacceptably, while elevated gelatin ratio resulted in increased viscosity that impaired the deposition process. With the optimal ratio of alginate to gelatin determined in this study, this hydrogel can be smoothly printed onto the platform and hold its shape until crosslinking via $CaCl_2$.

The duration time and shear stress in the extrusion process and syringe tip diameter can influence the cell viability.[53] The moderate extrusion environment and ionic crosslinking process ensured high cell viability compared to small syringe tip and chemical crosslink.[24,41] Both SMC and VIC showed high cell viability after encapsulated within the hydrogel discs (>90% for 1 day culture and >80% for 7 days). The slight decrease in cell number and overall viability over 7 day culture was likely due to some impairment of cell adhesion, which is commonly reported by other groups using alginate and other bioinert hydrogels such as poly (ethylene glycol) and hyaluronic acid.[44-46] Therefore, these 3D hydrogel constructs can maintain high cell viability with clinically relevant thickness.

The increase in cell spreading over culture was probably due to the temporal dissociation of alginate by gradual ion exchange process between Na^+ and Ca^{2+} ions,[39,47] and increased availability of gelatin. Recent studies have highlighted that VIC are a heterogeneous population, exhibiting a continuum of fibroblast and myofibroblast phenotypes.[48] In our study, the encapsulated VIC expressed both vimentin and αSMA (though significantly more vimentin), characteristic of a myofibroblast phenotype. It has been reported that VIC can activate to a myofibroblast in response to mechanically stiff and/or remodeling or diseased microenvironments[1,49]. Conversely, soft substrates promote fibroblast activity.[50] While the precise biomechanical thresholds for each have yet to be determined, the modulus of the alginate/gelatin hydrogels in future studies might need to be lowered for increased fibroblast phenotype.

The tensile stress and modulus of printed cell-free dumbbell-shaped hydrogel samples decreased with culture. This was likely caused by gradual dissociation via Na^+ and Ca^{2+} ion exchange and early release of gelatin (Fig. S1). The tensile stress and modulus of cell free printed hydrogel samples were comparable to those for non-calcified human aortic heart valve cusps (around 1.74±0.29 MPa for tensile stress and 1.98 ±0.15 MPa for modulus at the level of stress 1.0 MPa in radial direction. However, hydrogels encapsulated with VIC had

initially reduced tensile strength and failure strain compared to cell-free samples, probably due to the encapsulated cells that acted effectively like pores in the hydrogel samples. The encapsulated cells comprised a significant amount of the area of the hydrogels, but contributed minimally to the mechanics of the hydrogels when first deposited, as also reported previously with other hydrogels.[54] With increasing the culture time, the hydrogel alone decreased in stiffness and strength, while the cell-laden gels maintained them. The encapsulated VIC secreted their own extracellular matrix (ECM) including type I collagen, which likely compensated the effects of alginate dissociation and gelatin release. By day 7, the cell-laden constructs were approximately 40% less stiff than the initial cell-free scaffold, which our data suggests supported a largely (but not complete) fibroblastic VIC phenotype. It will be critical in future studies to include biomechanical heterogeneity as well as cellular heterogeneity in 3D printed valves (Laura ref). Changing the alginate to gelatin ratio can tune printed tissue mechanics, but the temperature around the hydrogel needs to be well controlled during printing in order to avoid premture gelation of gelatin. In addition, the chemical crosslinking performed in this study is a global process difficult to control and will limit the print time available. While smaller sized bioprinted valve conduits need less time for crosslinking, a similar decrease in spatial resolution will not reduce printing times. Photocrosslinking strategies may afford better control of tissue mechanics while not limiting the possible printing time. Inclusion of cell adhesion peptides and other biomacrolecules within the gel will likely improve cell viability, spreading, and proliferation. Further conduit culture within hemodynamic bioreactors can facilitate tissue remodeling and strengthening towards normal tissue architecture, likely an important step before future animal implantation studies (Sutherland 2007).

Conclusions

We establish a method to fabricate mechanically robust living tri-leaflet heart valves using 3D printing and multiple valve cell populations. The encapsulated VIC and SMC had high viability, good spreading, and phenotype retention in culture. 3D bioprinted cell encapsulated valve conduits are thus a promising strategy for tissue engineered living valve replacements.

Supplementary Material

Refer to Web version on PubMed Central for supplementary material.

Acknowledgments

This work was funded by the Morgan Family Foundation, The Hartwell Foundation, the National Science Foundation (CBET-0955172), and the American Heart Association (0830384N). We would like to thank Microscopy and Imaging Facility, Life Sciences Core Laboratories Center in Cornell University for their assistance with CLSM imaging.

References

1. Butcher JT, Mahler GJ, Hockaday LA. Aortic valve disease and treatment: The need for naturally engineered solutions. Adv Drug Deliv Rev. 2011; 63:242–268. [PubMed: 21281685]
2. Hinton RB, Yutzey KE. Heart Valve Structure and Function in Development and Disease. Annu Rev Physiol. 2011; 73:29–46. [PubMed: 20809794]
3. Filova E, Straka F, Mirejovsky T, Masin J, Bacakova L. Tissue-engineered heart valves. Physiol Res. 2009; 58:S141–S158. [PubMed: 20131932]
4. Vesely I. Heart valve tissue engineering. Circ Res. 2005; 97:743–755. [PubMed: 16224074]

5. Brown JW, Ruzmetov M, Rodefeld MD, Mahomed Y, Turrentine MW. Incidence of and risk factors for pulmonary autograft dilation after ross aortic valve replacement. Ann Thorac Surg. 2007; 83:1781–1789. [PubMed: 17462399]
6. Gandaglia A, Bagno A, Naso F, Spina M, Gerosa G. Cells, scaffolds and bioreactors for tissue-engineered heart valves: a journey from basic concepts to contemporary developmental innovations. Eur J Cardio-Thorac Surg. 2011; 39:523–531.
7. Sodian R, Hoerstrup SP, Sperling JS, Daebritz SH, Martin DP, Schoen FJ, Vacanti JP, Mayer JE. Tissue engineering of heart valves: *In vitro* experiences. Ann Thorac Surg. 2000; 70:140–144. [PubMed: 10921698]
8. Schmidt D, Dijkman PE, Driessen-Mol A, Stenger R, Mariani C, Puolakka A, Rissanen M, Deichmann T, Odermatt B, Weber B. Minimally-invasive implantation of living tissue engineered heart valves a comprehensive approach from autologous vascular cells to stem cells. J Am Coll Cardiol. 2010; 56:510–520. [PubMed: 20670763]
9. Tedder ME, Simionescu A, Chen J, Liao J, Simionescu DT. Assembly and testing of stem cell-seeded layered collagen constructs for heart valve tissue engineering. Tissue Eng Part A. 2011; 17:25–36. [PubMed: 20673028]
10. Sacks MS, Schoen FJ, Mayer JEJ. Bioengineering challenges for heart valve tissue engineering. Annu Rev Biomed Eng. 2009; 11:289–313. [PubMed: 19413511]
11. van Vlimmeren MAA, Driessen-Mol A, Oomens CWJ, Baaijens FPT. An in vitro model system to quantify stress generation, compaction, and retraction in engineered heart valve tissue. Tissue Eng Part C. 2011; 17:983–991.
12. Schaefermeier PK, Szymanski D, Weiss F, Fu P, Lueth T, Schmitz C, Meiser BM, Reichart B, Sodian R. Design and fabrication of three-dimensional scaffolds for tissue engineering of human heart valves. Eur Surg Res. 2009; 42:49–53. [PubMed: 18987474]
13. Sodian R, Schaefermeier P, Abegg-Zips S, Kuebler WM, Shakibaei M, Daebritz S, Ziegelmueller J, Schmitz CR, Reichart B. Use of human umbilical cord blood-derived progenitor cells for tissue-engineered heart valves. Ann Thorac Surg. 2010; 89:819–828. [PubMed: 20172137]
14. Flanagan TC, Cornelissen C, Koch S, Tschoeke B, Sachweh JS, Schmitz-Rode T, Jockenhoevel S. The in vitro development of autologous fibrin-based tissue-engineered heart valves through optimised dynamic conditioning. Biomaterials. 2007; 28:3388–3397. [PubMed: 17467792]
15. Courtney T, Sacks MS, Stankus J, Guan J, Wagner WR. Design and analysis of tissue engineering scaffolds that mimic soft tissue mechanical anisotropy. Biomaterials. 2006; 27:3631–3638. [PubMed: 16545867]
16. Sewell-Loftin MK, Chun YW, Khademhosseini A, Merryman WD. EMT-inducing biomaterials for heart valve engineering: Taking cues from developmental biology. J Cardiovasc Transl Res. 2011; 4:658–671. [PubMed: 21751069]
17. Cheng A, Dagum P, Miller DC. Aortic root dynamics and surgery: from craft to science. Philos Trans R Soc B-Biol Sci. 2007; 362:1407–1419.
18. Guillotin B, Guillemot F. Cell patterning technologies for organotypic tissue fabrication. Trends Biotechnol. 2011; 29:183–190. [PubMed: 21256609]
19. Mironov V, Reis N, Derby B. Bioprinting: A beginning. Tissue Eng. 2006; 12:631–634. [PubMed: 16674278]
20. Chang CC, Boland ED, Williams SK, Hoying JB. Direct-write bioprinting three-dimensional biohybrid systems for future regenerative therapies. J Biomed Mater Res Part B. 2011; 98B:160–170.
21. Cohen DL, Lo W, Tsavaris A, Peng D, Lipson H, Bonassar LJ. Increased mixing improves hydrogel homogeneity and quality of three-dimensional printed constructs. Tissue Eng Part C-Methods. 2011; 17:239–248. [PubMed: 20822480]
22. Skardal A, Zhang JX, Prestwich GD. Bioprinting vessel-like constructs using hyaluronan hydrogels crosslinked with tetrahedral polyethylene glycol tetracrylates. Biomaterials. 2010; 31:6173–6181. [PubMed: 20546891]
23. Li SJ, Xiong Z, Wang XH, Yan YN, Liu HX, Zhang RJ. Direct Fabrication of a hybrid cell/hydrogel construct by a double-nozzle assembling technology. J Bioact Compat Polym. 2009; 24:249–265.

24. Pescosolido L, Schuurman W, Malda J, Matricardi P, Alhaique F, Coviello T, van Weeren PR, Dhert WJA, Hennink WE, Vermonden T. Hyaluronic acid and dextran-based semi-IPN hydrogels as biomaterials for bioprinting. Biomacromolecules. 2011; 12:1831–1838. [PubMed: 21425854]
25. Elomaa L, Teixeira S, Hakala R, Korhonen H, Grijpma DW, Seppala JV. Preparation of poly(epsilon-caprolactone)-based tissue engineering scaffolds by stereolithography. Acta Biomater. 2011; 7:3850–3856. [PubMed: 21763796]
26. Ovsianikov A, Deiwick A, Van Vlierberghe S, Dubruel P, Moller L, Drager G, Chichkov B. Laser fabrication of three-dimensional CAD scaffolds from photosensitive gelatin for applications in tissue engineering. Biomacromolecules. 2011; 12:851–858. [PubMed: 21366287]
27. Censi R, Schuurman W, Malda J, di Dato G, Burgisser PE, Dhert WJA, van Nostrum CF, di Martino P, Vermonden T, Hennink WE. A printable photopolymerizable thermosensitive p(HPMAm-lactate)-PEG hydrogel for tissue engineering. Adv Funct Mater. 2011; 21:1833–1842.
28. Schuurman W, Khristov V, Pot MW, van Weeren PR, Dhert WJA, Malda J. Bioprinting of hybrid tissue constructs with tailorable mechanical properties. Biofabrication. 2011; 3:021001. [PubMed: 21597163]
29. Butcher JT, Nerem RM. Porcine aortic valve interstitial cells in three-dimensional culture: comparison of phenotype with aortic smooth muscle cells. J Heart Valve Dis. 2004; 13:478–486. [PubMed: 15222296]
30. Filho AL, Cheung PY, Noritomi PY, Silva JVL, Colangelo NW, Kang H, Lipson H, Butcher JT, Malone E, Neto PI. Construction and aaptation of an open source rapid prototyping machine for biomedical research purposes - a multinational collaborative development. Adv Res Virt Rapid Protyping. 2009
31. Hockaday LA, Kang KH, Colangelo NW, Cheung PYC, Malone E, Wu J, Girardi LN, Bonassar LJ, Lipson H, Chu CC. Solid freeform fabrication of living aortic valve conduits. Biofabrication. 2012
32. Mendez MG, Kojima SI, Goldman RD. Vimentin induces changes in cell shape, motility, and adhesion during the epithelial to mesenchymal transition. Faseb J. 2010; 24:1838–1851. [PubMed: 20097873]
33. Lu SH, Lin ATL, Chen KK, Chiang HS, Chang LS. Characterization of smooth muscle differentiation of purified human skeletal muscle-derived cells. J Cell Mol Med. 2011; 15:587–592. [PubMed: 20132408]
34. Stephens EH, Durst CA, West JL, Grande-Allen KJ. Mitral valvular interstitial cell responses to substrate stiffness depend on age and anatomic region. Acta Biomater. 2011; 7:75–82. [PubMed: 20624493]
35. Pohl HBF, Porcheri C, Mueggler T, Bachmann LC, Martino G, Riethmacher D, Franklin RJM, Rudin M, Suter U. Genetically induced adult oligodendrocyte cell death is associated with poor myelin clearance, reduced remyelination, and axonal damage. J Neurosci. 2011; 31:1069–1080. [PubMed: 21248132]
36. Khromova N, Kopnin P, Rybko V, Kopnin BP. Downregulation of VEGF-C expression in lung and colon cancer cells decelerates tumor growth and inhibits metastasis via multiple mechanisms. Oncogene. 2012; 31:1389–1397. [PubMed: 21804602]
37. Augst AD, Kong HJ, Mooney DJ. Alginate hydrogels as biomaterials. Macromol Biosci. 2006; 6:623–633. [PubMed: 16881042]
38. Wang N, Adams G, Buttery L, Falcone FH, Stolnik S. Alginate encapsulation technology supports embryonic stem cells differentiation into insulin-producing cells. J Biotechnol. 2009; 144:304–312. [PubMed: 19686786]
39. Lee KY, Mooney DJ. Alginate: Properties and biomedical applications Prog Polym Sci 2011;In press.
40. Guillemot F, Souquet A, Catros S, Guillotin B, Lopez J, Faucon M, Pippenger B, Bareille R, Remy M, Bellance S. High-throughput laser printing of cells and biomaterials for tissue engineering. Acta Biomater. 2010; 6:2494–2500. [PubMed: 19819356]
41. Khalil S, Sun W. Bioprinting endothelial cells with alginate for 3D tissue constructs. J Biomech Eng- Trans ASME. 2009:131.

42. Guillotin B, Souquet A, Catros S, Duocastella M, Pippenger B, Bellance S, Bareille R, Remy M, Bordenave L, Amedee J. Laser assisted bioprinting of engineered tissue with high cell density and microscale organization. Biomaterials. 2010; 31:7250–7256. [PubMed: 20580082]
43. Panouille M, Larreta-Garde V. Gelation behaviour of gelatin and alginate mixtures. Food Hydrocolloids. 2009; 23:1074–1080.
44. Chou AI, Nicoll SB. Characterization of photocrosslinked alginate hydrogels for nucleus pulposus cell encapsulation. J Biomed Mater Res Part A. 2009; 91A:187–194.
45. Elisseeff J, McIntosh W, Anseth K, Riley S, Ragan P, Langer R. Photoencapsulation of chondrocytes in poly(ethylene oxide)-based semi-interpenetrating networks. J Biomed Mater Res. 2000; 51:164–171. [PubMed: 10825215]
46. Chung C, Burdick JA. Influence of three-dimensional hyaluronic acid microenvironments on mesenchymal stem cell chondrogenesis. Tissue Eng Part A. 2009; 15:243–254. [PubMed: 19193129]
47. Bajpai SK, Sharma S. Investigation of swelling/degradation behaviour of alginate beads crosslinked with Ca^{2+} and Ba^{2+} ions. Reactive & Functional Polymers. 2004; 59:129–140.
48. Butcher JT, Simmons CA, Warnock JN. Review - Mechanobiology of the aortic heart valve. J Heart Valve Dis. 2008; 17:62–73. [PubMed: 18365571]
49. Aikawa E, Whittaker P, Farber M, Mendelson K, Padera RF, Aikawa M, Schoen FJ. Human semilunar cardiac valve remodeling by activated cells from fetus to adult - Implications for postnatal adaptation, pathology, and tissue engineering. Circulation. 2006; 113:1344–1352. [PubMed: 16534030]
50. Kloxin AM, Benton JA, Anseth KS. In situ elasticity modulation with dynamic substrates to direct cell phenotype. Biomaterials. 2010; 31:1–8. [PubMed: 19788947]
51. Maher PS, Keatch RP, Donnelly K, Mackay RE, Paxton JZ. Construction of 3D biological matrices using rapid prototyping technology. Rapid Prototyping J. 2009; 15:204–210.
52. Fedorovich NE, Wijnberg HM, Dhert WJA, Alblas J. Distinct tissue formation by heterogeneous printing of osteo- and endothelial progenitor cells. Tissue Eng Part A. 2011; 17:2113–2121. [PubMed: 21513466]
53. Cheng J, Lin F, Liu HX, Yan YN, Wang XH, Zhang R, Xiong Z. Rheological properties of cell-hydrogel composites extruding through small-diameter tips. J Manuf Sci Eng-Trans ASME. 2008; 130:021014.
54. Durst CA, Cuchiara MP, Mansfield EG, West JL, Grande-Allen KJ. Flexural characterization of cell encapsulated PEGDA hydrogels with applications for tissue engineered heart valves. Acta Biomater. 2011; 7:2467–2476. [PubMed: 21329770]
55. Visconti RP, Kasyanov V, Gentile C, Zhang J, Markwald RR, Mironov V. Towards organ printing: engineering an intra-organ branched vascular tree. Expert Opin Biol Ther. 2011; 10:409–420. [PubMed: 20132061]

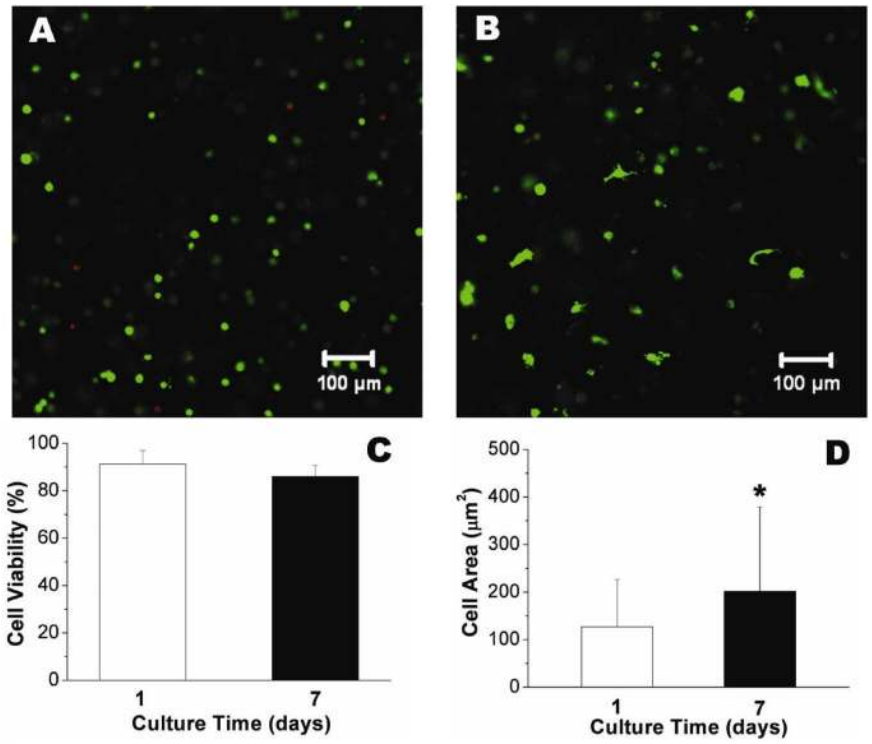

Figure 1.

Live/Dead assay for encapsulated VIC within alginate/gelatin hydrogel discs. (A) 1 day; (B) 7 days; (C) cell viability measured based on Live/Dead images; (D) average cell area measured based on Live/Dead images. (n=6, $*p < 0.05$)

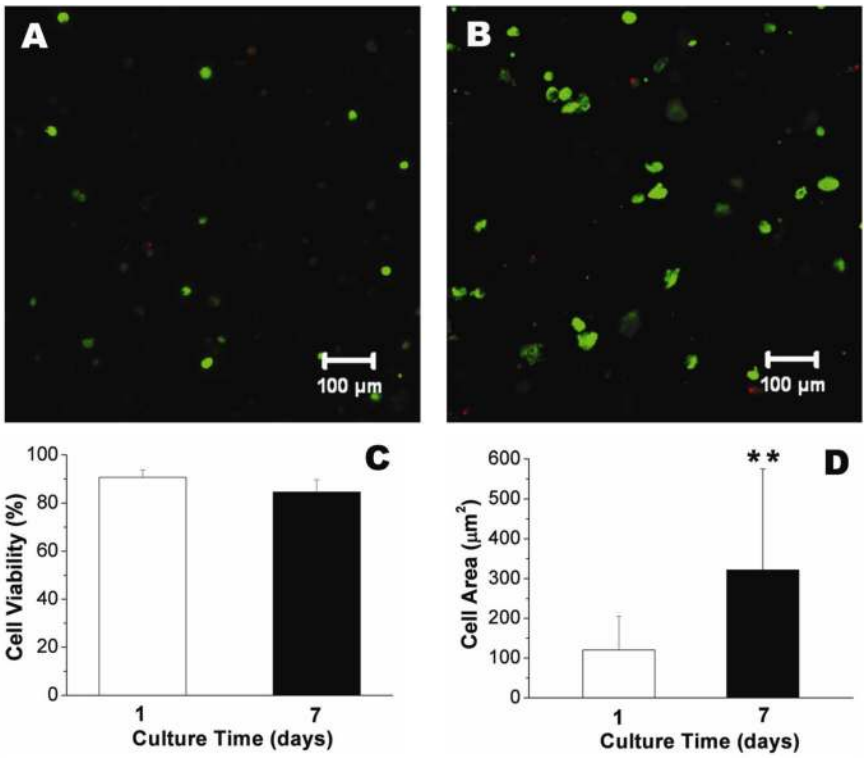

Figure 2.

Live/Dead assay for encapsulated SMC within alginate/gelatin hydrogel discs. (A) 1 day; (B) 7 days; (C) cell viability measured based on Live/Dead images; (D) average cell area measured based on Live/Dead images. (n=6, $*p < 0.05$)

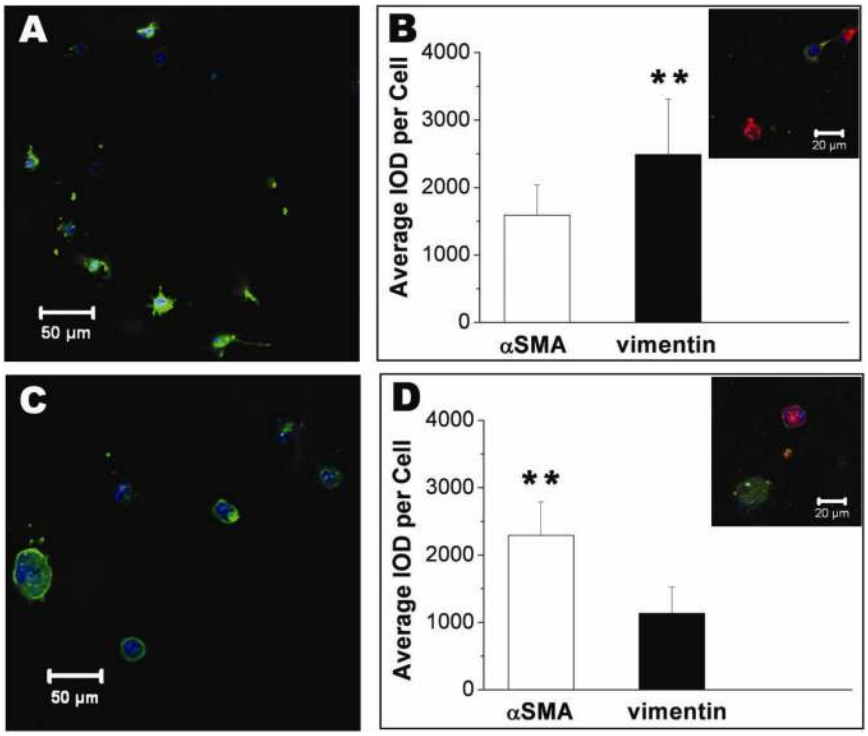

Figure 3.

Fluorescent staining for encapsulated VIC and SMC after 7 day culture. (A, C) Alexa Fluor 488 conjugated phalloidin staining for F-actin (green) and Draq 5 counterstaining for cell nuclei (blue); (B, D) αSMA and vimentin staining intensity for encapsulated VIC and SMC within hydrogel discs. (inset: representative image of immunohistochemical staining for αSMA (green) and vimentin (red), and Draq 5 counterstaining for cell nuclei (blue), n=6, $^{**}p<0.01$). (A, B) Encapsulated VIC; (C, D) encapsulated SMC.

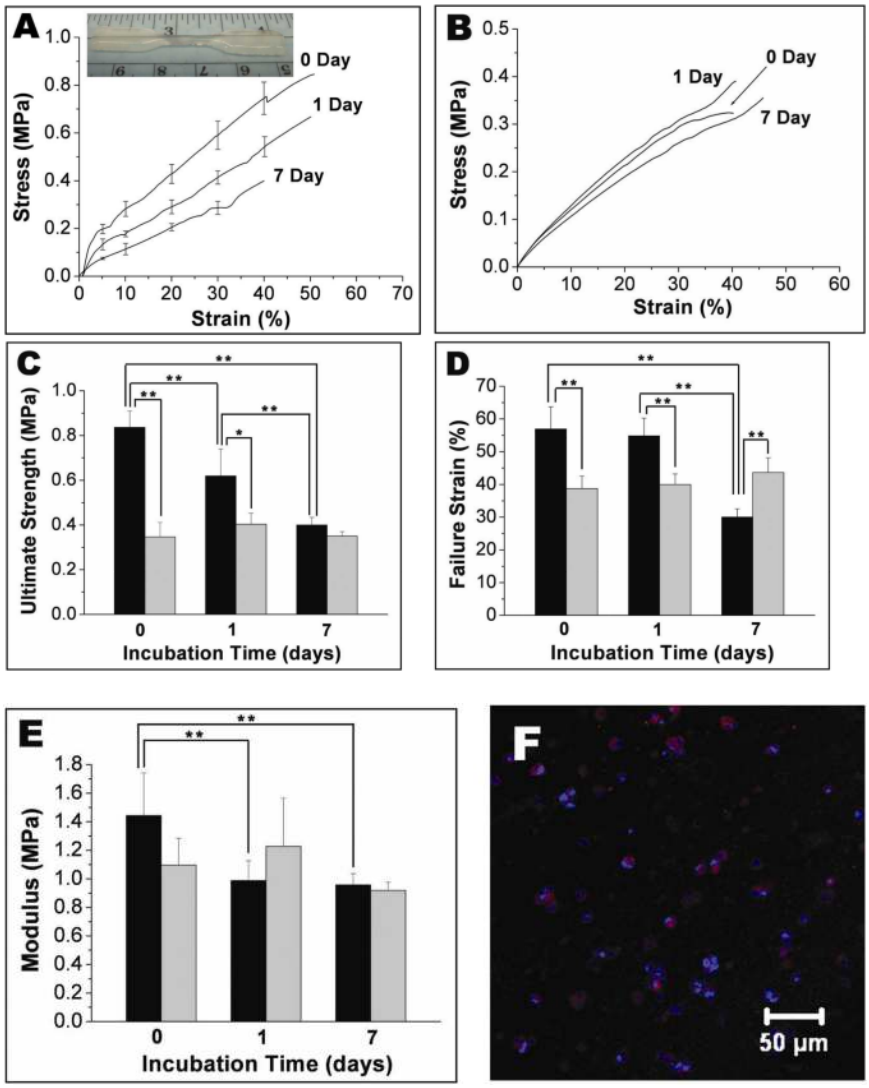

Figure 4.

Hydrogel tensile biomechanics. (A) Stress-strain curves of alginate/gelatin samples after incubation in culture medium (inset: as-printed alginate/gelatin hydrogel sample for tensile test); (B) Typical stress-strain curves of alginate/gelatin samples encapsulated with VIC; (C) change of ultimate strength with incubation time; (D) change of failure strain with incubation time (black column: cell-free hydrogel samples; gray column: cell laden hydrogel samples); (E) change of modulus with incubation time; (black column: cell-free hydrogel samples; gray column: cell laden hydrogel samples; n=4-6 for cell-free hydrogel samples, n=3 for cell-laden hydrogel samples; *p<0.05, **p<0.01) (F) immunohistochemical staining of VIC encapsulated dumbbell shaped hydrogel sample for Col1A2 (red) and Draq 5 counterstaining for cell nuclei after 7 day culture (blue).

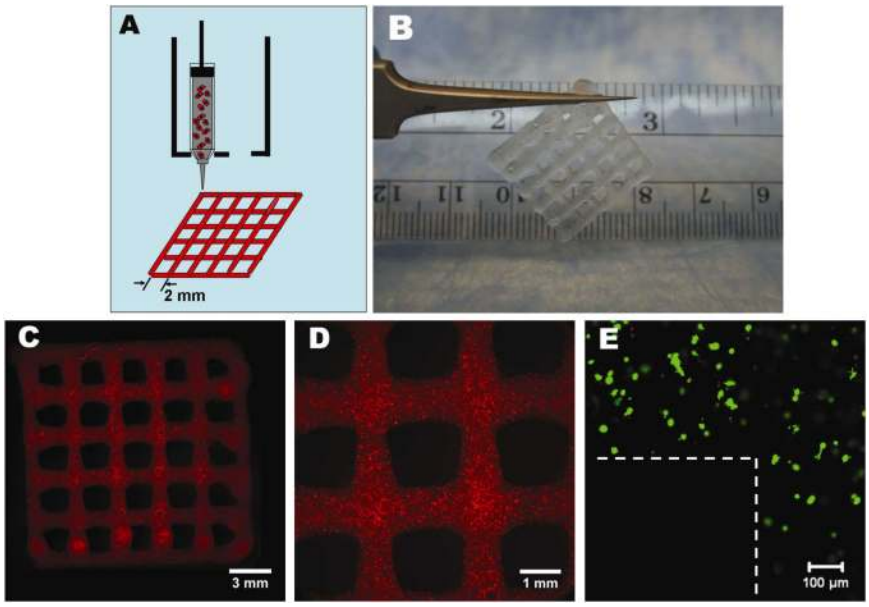

Figure 5.

Bioprinting of 3D grid pattern structure. (A) Schematic illustration of the bioprinting process with single cell type and single syringe; (B) bioprinted alginate/gelatin hydrogel structure after ionic crosslinking; (C) fluorescent image of printed 2D structure with encapsulation of cell tracker red labeled VIC; (D) close view of (C); (E) Live/Dead staining of VIC within bioprinted hydrogel after 7 days culture (the dashed line indicates the pore area).

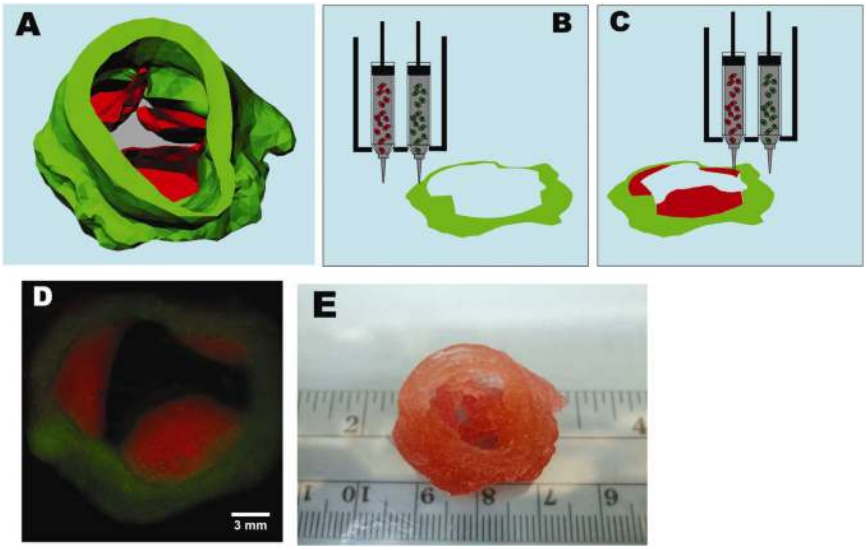

Figure 6.

Bioprinting of aortic valve conduit. (A) Aortic valve model reconstructed from micro-CT images. The root and leaflet regions were identified with intensity thresholds and rendered separately into 3D geometries into STL format (green color indicates valve root and red color indicates valve leaflets); (B, C) schematic illustration of the bioprinting process with dual cell types and dual syringes; (B) root region of first layer generated by hydrogel with SMC; (C) leaflet region of first layer generated by hydrogel with VIC; (D) fluorescent image of first printed two layers of aortic valve conduit; SMC for valve root were labeled by cell tracker green and VIC for valve leaflet were labeled by cell tracker red. (E) as-printed aortic valve conduit.

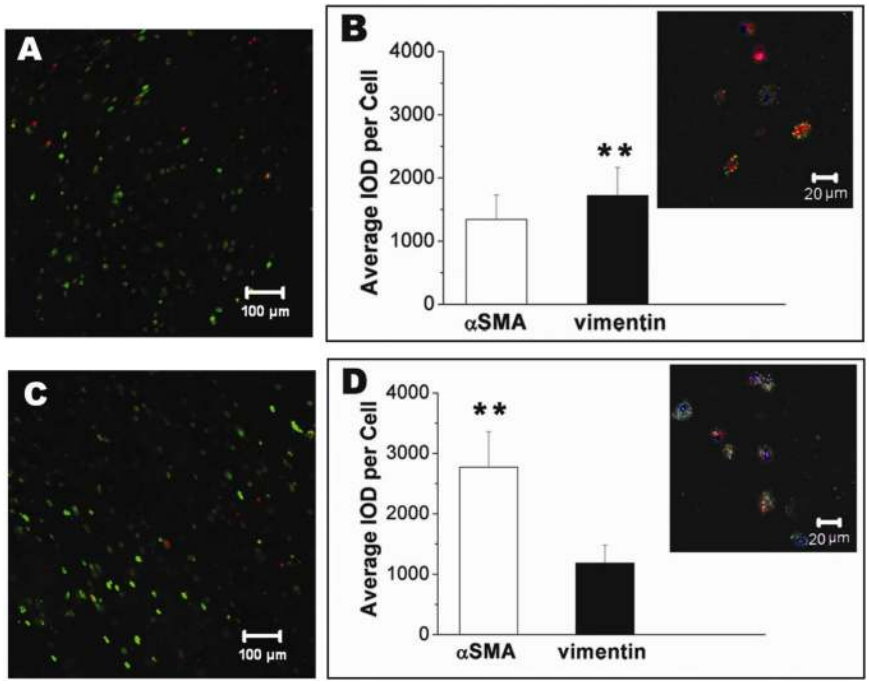

Figure 7.

Fluorescent staining for bioprinted aortic valve conduit with encapsulation of VIC and SMC after 7 day culture. (A, C) Live/Dead assay for encapsulated VIC in the leaflet and SMC in valve root after 7 day culture; (B, D) αSMA and vimentin staining intensity for encapsulated VIC and SMC within the bioprinted conduit. (inset: representative image of immunohistochemical staining for αSMA (green) and vimentin (red), and Draq 5 counterstaining for cell nuclei (blue), n=6, $^{**}p<0.01$). (A, B); staining for VIC in the leaflet; (C, D) staining for SMC in the root.